Microstructure and inter-grain magnetoresistance in Ag-doped polycrystalline $La_{0.67}Sr_{0.33}MnO_3$ thin films

2002 J. Phys.: Condens. Matter 14 6341

(http://iopscience.iop.org/0953-8984/14/25/304)

INSTITUTE OF PHYSICS PUBLISHING JOURNAL OF PHYSICS: CONDENSED MATTER

J. Phys.: Condens. Matter **14** (2002) 6341–6351 PII: S0953-8984(02)35657-1

Microstructure and inter-grain magnetoresistance in Ag-doped polycrystalline $La_{0.67}Sr_{0.33}MnO_3$ thin films

J Li[1,3], C K Ong[1], Q Zhan[2] and D X Li[2]

[1] Centre for Superconducting and Magnetic Materials (CSMM) and Department of Physics, National University of Singapore, 2 Science Drive 3, 117542, Singapore
[2] Shenyang National Laboratory for Materials Science, Institute of Metal Research, Chinese Academy of Sciences, 72 Wenhua Road, Shenyang 110016, China

E-mail: ieslijie@nus.edu.sg (J Li)

Received 9 April 2002, in final form 21 May 2002
Published 14 June 2002
Online at stacks.iop.org/JPhysCM/14/6341

Abstract

Ag-doped $La_{0.67}Sr_{0.33}MnO_3$ thin films with various Ag concentrations were deposited on (001) $LaAlO_3$ substrates at 400 °C by using a dual-beam pulsed-laser deposition system. The Ag-doped films show polycrystalline structure with epitaxial *c*-axis columns. These columns were composed of closely arranged polyhedra of size 10–15 nm, resulting from the enhanced stress-induced grain boundary diffusion. In the case of heavy doping, tiny separated Ag crystals were observed at grain boundaries. Due to the interaction between the two laser-induced plumes, the Ag precipitation also helped to form anomalous clusters consisting of nano-sized grains and amorphous phase. By adjusting the deposition conditions carefully, we can tailor the microstructure of the film and correspondingly alter the resistivity and the inter-grain magnetoresistance of the Ag-doped films. Theoretical simulation led to results consistent with the microstructure observations and the magnetoresistance measurements.

1. Introduction

For the $YBa_2Cu_3O_{7-\delta}$ (YBCO) superconducting system (perovskite materials), the effect of Ag doping has been widely investigated [1–3]. Previous results show that, firstly, there is no chemical reaction between the Ag and the YBCO lattice. Most researchers believe that Ag cannot be substituted into the lattice; that, on the contrary, it only diffuses to grain boundaries or other defects. Secondly, Ag dopant exists in the form of a metal instead of insulating oxides. Thirdly, Ag doping can improve the crystallinity of the epitaxial YBCO films, most probably by providing extra oxygen to the lattice. Finally, due to the rapid diffusion of Ag on the film/substrate interface, the diffusion of the lattice atoms is accelerated and the grain size in the Ag-doped samples is generally larger. Therefore, Ag has long been used to dope YBCO to enhance the critical current J_c [3].

[3] Author to whom any correspondence should be addressed.

Correspondingly, research on Ag-doped manganites, another perovskite material, has been reported only by a few groups [4–6]. Indirect evidence of the doping effect in epitaxial manganite films has been provided, and conclusions consistent with those from previous studies of YBCO have been presented. However, change of the magnetoresistive (MR) behaviour with Ag concentration in the $LaMnO_3$ system has been reported recently, and it has been argued that substitution of Ag into the La site of the manganites occurs [7]. It is then of interest to find out whether the MR change observed in the manganites originates from the La-site substitution of Ag, or from the modification of the grain boundary conditions due to the presence of the Ag.

In this paper we attempt to explore the effect of Ag doping on the microstructure and MR phenomenon in polycrystalline $La_{0.67}Sr_{0.33}MnO_3$ (LSMO) thin films. A direct observation of the doping effect on grain boundaries has been achieved by transmission electron microscopy (TEM). Combined with magnetotransport property measurements and simulation, our experiments reveal that the role of Ag in the LSMO films is mainly that of catalysing the grain boundary diffusion of LSMO species, and thus improving the grain boundary ordering.

2. Experimental details

The stoichiometric ceramic LSMO target was sintered using the conventional solid-state reaction at 1300 °C in air. A metal Ag target was used for doping. LSMO and Ag were co-deposited on (001) $LaAlO_3$ (LAO) single-crystal substrates at 400 °C. Details of the dual-beam pulsed-laser deposition (DBPLD) experimental facilities have been given previously [3, 5, 6, 8]. While the frequency of the laser beam incident on the manganite target was fixed at 4 Hz, that on the Ag target could be adjusted using a chopper from 0 to 8 Hz. The Ag precipitation during deposition, and consequently the Ag concentration in the film, could then be changed. After deposition, the films were annealed *in situ* for 1 h before being cooled down slowly. A fixed oxygen pressure of 0.2 mbar was introduced during the deposition and the post-annealing procedure. The thicknesses of all the thin films were around 150 nm, and the in-plane dimension was 5×10 mm^2.

The choice of single-crystalline rather than polycrystalline LAO for the substrates is based on the fact that epitaxial LSMO film is expected to appear on LAO single crystals once the deposition temperature T_s is appropriate, and at lower T_s, column-like grains will grow epitaxially from the substrate and span the whole film thickness, as we will describe in the next section. Therefore a three-dimensional study on the grain size, shape, as well as grain boundary thickness and orientation can be simplified into a two-dimensional plan-view observation.

The film microstructure was determined by using fine-step x-ray diffraction (XRD), TEM, and high-resolution TEM (HRTEM). The temperature dependences of the film resistivity and the MR were studied using a conventional four-probe technique over a temperature range of 78–330 K. Four Au electrodes were deposited on the film surface using a metal mask by an electron-beam evaporation system. The electrodes were 1.5 mm in width and 5 mm in length, across the width of the film. The relatively low resistivity of Au can help to distribute the measuring current evenly in the film plane.

3. Experimental results and discussion

3.1. Microstructure characterization

The x-ray spectra of all the samples show only (00*l*) peaks of LSMO in addition to peaks contributed from the substrate. No reflection of Ag or any of the Ag compounds is detectable, despite the occurrence of Ag precipitation during film deposition. The above-mentioned experimental results reveal that the films have *c*-axis texture, and that the Ag dopant, if it is present, must be so only in small amounts. This is most probably due to the extremely high saturation pressure of Ag at the film deposition temperatures [1, 5, 6, 9]. No doping-induced lattice parameter change is identified.

Cross section TEM studies reveal a column-like microstructure in films deposited at $T_s = 400\,^{\circ}$C, as shown in figure 1(a). These columns grow epitaxially from the substrate and span the entire 120 nm thickness of the film. Impurities, amorphous phase, pores, and other disordered structures exist at the interfaces among these columns. Therefore films deposited at this temperature are polycrystalline. Figure 1(b) is the planar section TEM image of the sample deposited at 400 °C with Ag precipitation at 3 Hz. It is clear that the film consists of columns of about 10–15 nm, with some scattered anomalous larger grains of about 50–100 nm. The inset selected-area electron diffraction pattern in figure 1(b) is a polycrystalline pattern, but the sign of the in-plane alignment is still dominant. However, it is interesting to note that there is also a fraction of amorphous phase existing in the sample, as deduced from the diffusive halo in the diffraction pattern. We also note that, for the undoped sample, the diffraction pattern suggests weaker in-plane orientation, yet less amorphous phase. Correspondingly, while the anomalous larger grains are absent in the stoichiometric film, the content of these grains increases with increasing Ag precipitation in the Ag-doped films. Therefore, it is reasonable to claim that these larger grains are mixtures of nano-sized crystals and a high fraction of amorphous phase, formed due to Ag doping.

The HREM investigation for the films with and without Ag doping gives interesting results, as shown in figures 2(a) and (b). Figure 2(a) shows regular polygon-shaped grains of similar size, which are closely arranged, forming a honeycomb-like structure. Careful investigation shows that these grains, or columns, not only grow epitaxially along the *c*-axis, but also are almost aligned in the *ab*-plane, so the boundaries among these grains are of the small-angle type, and their thicknesses are only about 1 nm. This is consistent with the previously mentioned electron diffraction results shown in the inset of figure 1(b). A boot-shaped Ag crystalline grain with its [110] direction perpendicular to the film surface is observed, bounded by five LSMO grains. The size of the Ag grain is about 8 nm. This Ag grain is believed to be separated out during the film deposition and the 1 h post annealing procedure. On comparing with the microstructure of the undoped film shown in figure 2(b), the Ag doping effect on grain boundaries in the LSMO films is clear. In this undoped film, the shape of the LSMO grains is irregular and the grain sizes are dissimilar. The grain boundaries are much wider than those in the Ag-doped films: up to 3 nm.

We can then argue that: during film deposition and the post-annealing, the Ag dopant inside LSMO grains diffuses to the grain boundaries and then diffuses along the grain boundary to accumulate at the pores among the grains. At low temperature (as compared to the melting point), the grain boundary diffusion is dominant as compared with the intra-grain diffusion [10]. This Ag dopant then acts as a ‘catalyst’ and enhances the grain boundary diffusion of the LSMO lattice species. As illustrated in figure 3, due to the lattice mismatch between the LSMO and the LAO substrate, the film is subject to a compressive stress. A net diffusional atom current along the grain boundaries is then obtained, driven by the stress. The polycrystalline grains change their shape in response to the stress, which is the reason for the closely arranged honeycomb-like structure. Comparing figures 2(a) and (b), it is clear that, in the Ag-doped films, the dominant effect of Ag doping is to enhance the grain boundary diffusion, whereas the grain size enlargement effect can be ignored.

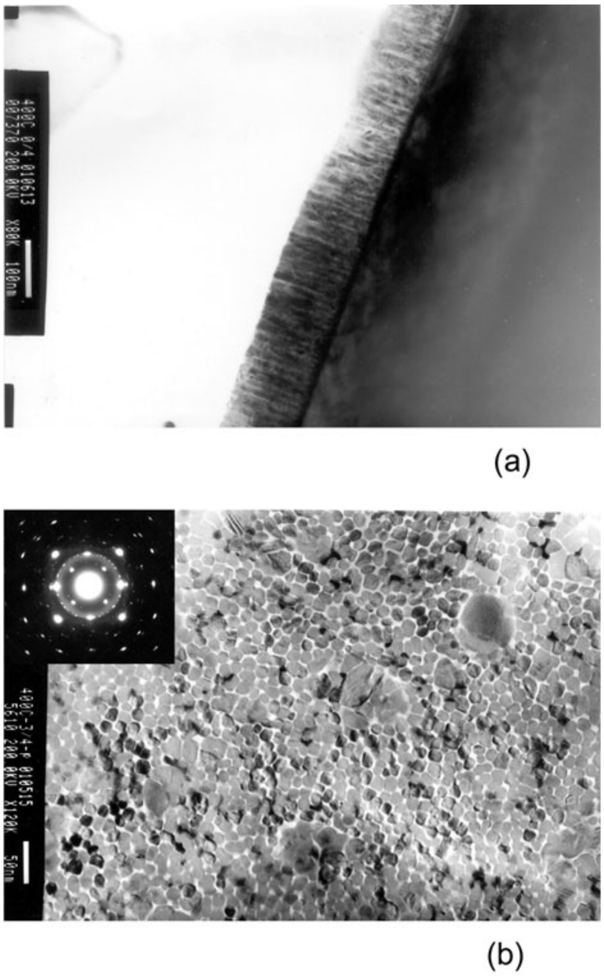

Figure 1. (a) The cross section TEM image of the stoichiometric LSMO film deposited on an LAO substrate at 400 °C. Column-like polycrystalline structure is shown. (b) The planar section TEM image of the film deposited under similar conditions but with Ag precipitation at 3 Hz. The size of the columns is about 10–15 nm. Anomalous larger grains scatter in the film. The inset shows the selected-area electron diffraction pattern.

3.2. Transport properties and the two-channel model

Our transport measurement gives results consistent with the microstructure observations. Figure 4(a) exhibits the dependence on temperature (T) of the sample resistance (R) for the films deposited at 400 °C with different Ag precipitations. The labels in the figure stand for the respective frequency ratios of the laser incident on the Ag and the LSMO target. A higher frequency ratio means more Ag precipitation during deposition. Figure 4(b) shows the MR values measured in a field of 4 kOe for the samples with Ag precipitation at 0, 1, 3, and 8 Hz. As we can see, the undoped film behaves like a metal from 77 to 330 K, and shows a small bulge in the ρ–T curve around room temperature, indicating the insulator-to-metal transition. This transition temperature is lower than the value for single crystals or epitaxial thin films (~365 K), due to the decoupling effect of grain boundaries in this polycrystalline sample.

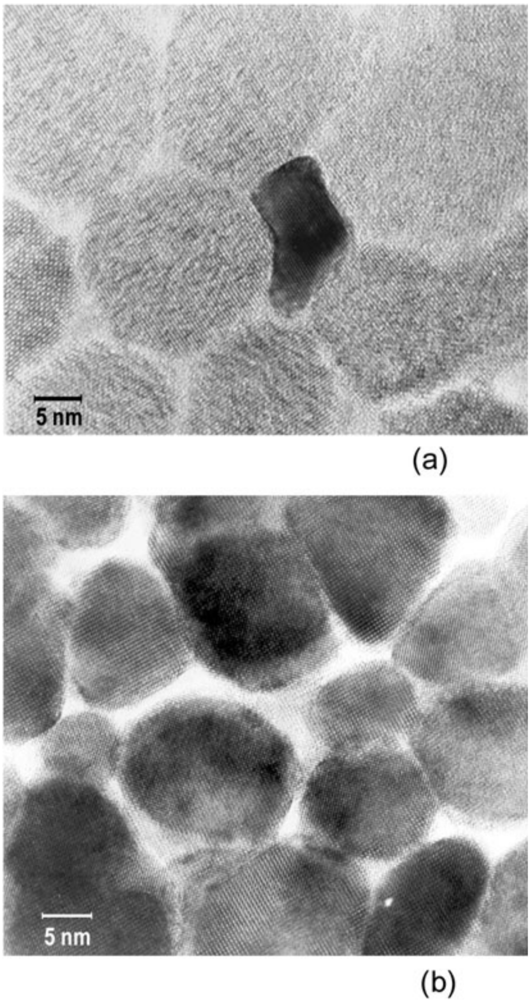

Figure 2. (a) The HREM planar section for the film deposited on an LAO substrate at 400 °C with Ag precipitation at 3 Hz. The polygonal grains are columns grown epitaxially from the substrate. The dark boot-shaped grain is an Ag nano-crystal of 8 nm. (b) The HREM planar section for the stoichiometric film deposited under similar conditions.

Accordingly, the $\Delta\rho/\rho$ value of the undoped film, shown in figure 4(b), is very low around the transition temperature, but increases with decreasing temperature. The fairly high MR value at low temperatures originates from the magnetic spin disordering in grain boundary regions, which attests to the granular nature of the film [11–15]. The $\Delta\rho/\rho$–H hysteresis loop measured at 77 K is presented in the inset of figure 4(b), where the MR response to the magnetic field H shows two distinct parts; this is a feature of an inter-grain-type MR.

With Ag precipitation at 1 Hz, the R–T curve remains approximately the same shape as the undoped one but is shifted downwards, indicating a reduced scattering of the conducting carriers, and thus a reduced content of lattice defects or an improved crystallinity in the film. Our earlier experiments on Ag-doped epitaxial films, however, have shown that Ag doping can only slightly change the magneto-electrical properties inside grains [5, 6]. Referring to the

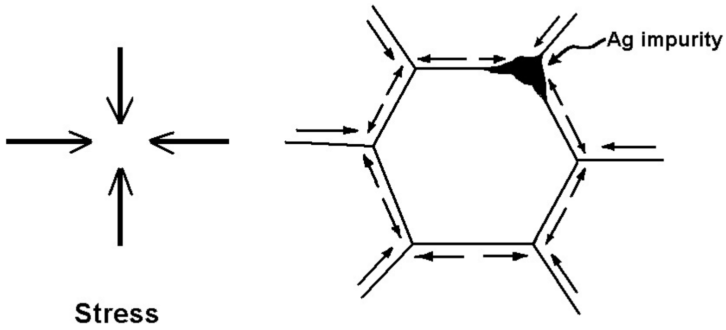

Figure 3. An illustration of the stress-induced diffusion current established along the grain boundaries in the polycrystalline LSMO films.

corresponding $\Delta\rho/\rho$ value, which is greatly suppressed at low temperatures as compared with that of the undoped case, one can conclude that the enhanced conductance results from an improved grain boundary ordering due to Ag doping, as has been evidenced by the microstructure evaluation. With Ag precipitation at 2 and 3 Hz, however, the sample resistance starts to increase slightly, although the further suppressed low-temperature $\Delta\rho/\rho$ value (see figure 4(b)) suggests an even more improved grain boundary ordering. As we can see, the increase in R is more obvious at high temperatures. The R–T curve for the film deposited with Ag precipitation at 3 Hz has a larger slope; consequently its low-temperature value is even lower than that of the film with Ag precipitation at 1 Hz. Furthermore, when the Ag precipitation is further increased, at up to 4 and 8 Hz, the film resistance decreases again. However, the $\Delta\rho/\rho$–T curve of sample '8/4' is almost superimposed on that of sample '3/4', which reveals that further increase in the Ag precipitation does not further improve the grain boundaries. Therefore, factors other than the grain boundary conditions must be affecting the sample resistance.

To achieve further understanding of the relationship between the magneto-electrical conduction behaviour and the microstructure in our Ag-doped films, we proposed a modified two-channel model [16, 17]. In this model the polycrystalline LSMO films are considered as composites where small crystal grains are separated by grain boundaries, amorphous phase, Ag-based impurities, and other defects. The grains, all connected by small-angle grain boundaries, form a conducting channel, which shows transport behaviour similar to that of an epitaxial film. That is, the behaviour is that of a metal over the whole temperature range that we investigated. The grains separated by large-angle grain boundaries or amorphous phase form an insulating channel. The overall resistance of this channel is mainly contributed by these energy barriers, whereas the contribution from the grains is negligible. These two channels align in parallel for electrotransport, and then the sample resistivity can be calculated from the following equation:

$$\frac{1}{\rho_s} = \frac{m}{\rho_c} + \frac{n}{\rho_i} \tag{1}$$

where m and n are the normalized section fractions for the conducting and the insulating channel respectively, and $n = 1 - m$.

Below T_c, the temperature dependence for an epitaxial LSMO film has been successfully given by [18, 19]

$$\rho_c = \rho_{c0} + \rho_{c2}T^2 + \rho_{c4.5}T^{4.5}. \tag{2}$$

Here the ρ_{c0} is the residual resistivity as $T \to 0$, and is inversely proportional to the defect density in the sample. The quadratic temperature dependence arises from the single-magnon

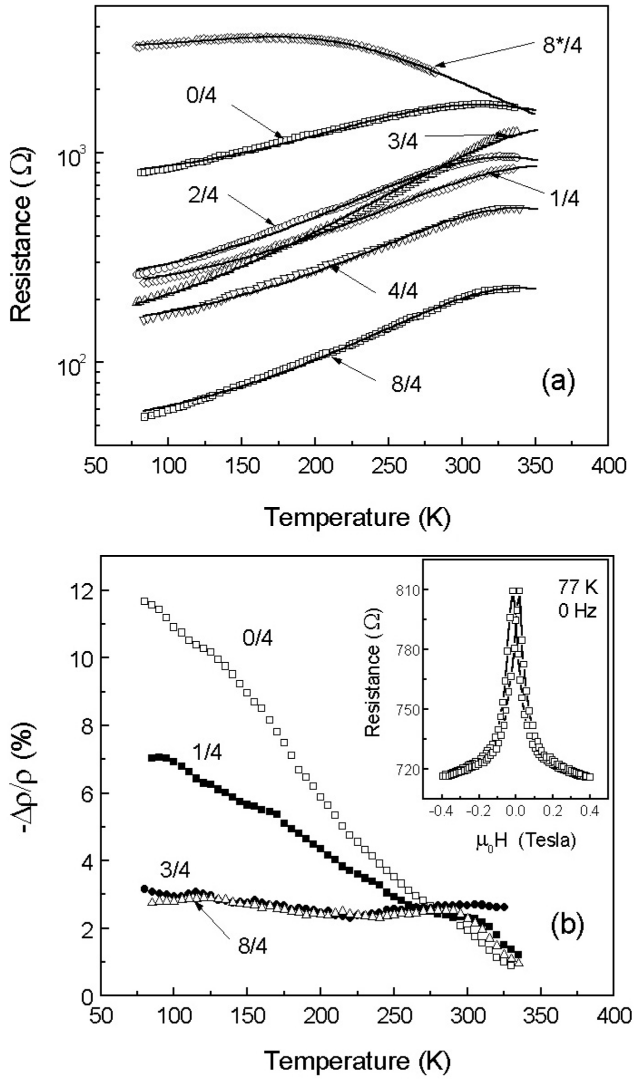

Figure 4. (a) The temperature-dependent sample resistance for the films deposited on LAO substrates at 400 °C. Fraction labels in the figure stand for the respective frequency ratios of the laser incident on the Ag and the LSMO target. The curve labelled as '8*/4' is explained in the text. The solid curves are simulation results obtained using the two-channel model. (b) The corresponding $\Delta\rho/\rho$ (4 kOe) values for the films deposited with Ag precipitations at 0, 1, 3, and 8 Hz. The inset shows the MR hysteresis loop for the undoped film, measured at 77 K.

scattering process, while the 4.5 term is due to the 100% polarized, two-magnon scattering process [18]. We fit the ρ–T curve (not shown here) of a stoichiometric epitaxial film deposited at 750 °C, and obtained the coefficients as

$$\begin{aligned} \rho_{c0} &= 0.17\ (\mathrm{m}\Omega\ \mathrm{cm}) \\ \rho_{c2} &= 9.5 \times 10^{-6}\ (\mathrm{m}\Omega\ \mathrm{cm}\ T^{-2}) \\ \rho_{c4.5} &= 5.48 \times 10^{-12}\ (\mathrm{m}\Omega\ \mathrm{cm}\ T^{-4.5}). \end{aligned} \tag{3}$$

On the other hand, the temperature dependence for the insulating channel can be expressed

Table 1. Fitting parameters for the films deposited with different Ag precipitations using the two-channel model. $m\%$ is the effective section fraction for the conducting channel (crystal grains connected by small-angle grain boundaries). ρ_{c0} (mΩ cm) is the residual resistivity as $T \to 0$ inside grains. E_a is the activation energy for the insulating channel (grain boundaries and/or the amorphous phase). ρ_{i0} (mΩ cm) is the resistivity as $T \to \infty$ for the insulating channel.

Ag doping	$m\%$	ρ_{c0} (mΩ cm)	E_a (eV)	ρ_{i0} (mΩ cm)
0/4	2.27 ± 0.02	0.88 ± 0.01	0.283 ± 0.007	1.4 ± 0.2
1/4	5.70 ± 0.03	0.645 ± 0.005	0.39 ± 0.02	0.24 ± 0.09
2/4	4.06 ± 0.03	0.500 ± 0.007	0.38 ± 0.08	0.20 ± 0.06
3/4	3.89 ± 0.04	0.312 ± 0.008	0.5 ± 0.1	(0.12)[a]
4/4	8.48 ± 0.05	0.640 ± 0.006	0.49 ± 0.02	0.023 ± 0.008
8/4	19.7 ± 0.1	0.511 ± 0.006	0.52 ± 0.02	0.006 ± 0.002
8*/4[b]	1.13 ± 0.04	1.78 ± 0.06	0.208 ± 0.003	2.9 ± 0.2

[a] Unreliable due to the lack of high-temperature data.
[b] The asterisk denotes the sample deposited, as the two laser plumes were very close.

using a simple band-gap model:

$$\rho_i = \rho_{i0} \exp\left(\frac{E_a}{2k_B T}\right) \tag{4}$$

where E_a is the activation energy and ρ_{i0} is the resistivity as $T \to \infty$.

Substituting equations (2) and (4) into (1), one obtains

$$\frac{1}{\rho_s} = \frac{m}{\rho_{c0} + \rho_{c2}T^2 + \rho_{c4.5}T^{4.5}} + \frac{1-m}{\rho_{i0}\exp(\frac{E_a}{2k_B T})}. \tag{5}$$

When fitting the data for Ag-doped samples using equation (5), we deliberately fixed the last two coefficients in ρ_c as the data shown in (3) and left ρ_{c0} free to reflect the crystallinities of the different samples. Therefore, four parameters, m, ρ_{c0}, $E_a/2k_B$, and $(1-m)/\rho_{i0}$ can be obtained by best fitting with (5). The results are listed in table 1, and the simulation curves are plotted in figure 4 as solid curves. It is obvious that the calculated curves fit the experimental data well.

Investigating table 1 carefully we find that, firstly, with Ag doping, the effective conducting section fraction $m\%$ is more than doubled, reflecting improved inter-grain connections or more ordered grain boundaries. This is consistent with the previously mentioned microstructure observations and transport behaviour analysis. This value decreases slightly as the Ag precipitation is further increased, to that at up to 2 and 3 Hz, corresponding to the slight increase in resistance at high temperatures for the two samples. Careful microstructure examination shows that the resistance increase is a result of the appearance of the anomalous larger grains, which contain a high fraction of amorphous phase, as revealed by the selected-area electron diffraction pattern shown in figure 1(b). The resistance increase due to the anomalous grains is more obvious in high-temperature regions. The reason for this is that at low temperatures the sample resistance is dominated by the grain boundary resistance, or the insulating channel. The very high values of $m\%$ found for the '4/4' and '8/4' samples are possibly a consequence of the metallic Ag separated out at grain boundaries. Although the increased number of anomalous grains tends to reduce $m\%$, the metallic Ag grains may form easier conducting paths, due to the percolation effect [20], thus reducing the overall resistance.

Secondly, the residual resistivity ρ_{c0} in these polycrystalline films is higher than that in epitaxial films. In other words, the grains formed at a fairly low T_s bear a relatively higher defect density. ρ_{c0} decreases with increasing Ag precipitation, indicating improved crystallinity due to Ag doping. As the Ag precipitation is further increased the value of ρ_{c0} starts to increase again. We may conclude that an appropriate amount of Ag doping benefits the crystallinity of LSMO, but a very high degree of Ag precipitation disturbs the deposition procedure and results in poor crystallinity.

Thirdly, for the insulating channel, the activation energy E_a increases while ρ_{i0} decreases monotonically with the Ag precipitation. One may note that the values of E_a and ρ_{i0} that we obtained vary fairly widely, and ρ_{i0} for sample '3/4' even varies by more than 100%. We believe that the lower reliability of the data for the insulating channel is due to our lack of high-temperature data. The highest temperature that we can reach is only 350 K. It is clear that, with the occurrence of Ag precipitation during film deposition, a phase with a higher energy barrier forms. We believe that it is the amorphous phase.

3.3. Other factors affecting the doping effect

However, in another series of experiments where the Ag precipitation was fixed as that at 8 Hz and the substrate temperature T_s was varied from 350 to 550 °C, we obtained results apparently contradicting those given above. Inter-grain MR enhancements were observed at nominally $T_s = 400$ and 450 °C, as reported in [5, 6]. The R–T curve for the Ag-doped film deposited at 400 °C in this series is also plotted in figure 4(a), labelled as '8*/4'. Comparing the '8*/4' curve with the curve labelled '8/4' for the film deposited with the same Ag precipitation and similar T_s, it is clear that the resistance of the former is much higher. The '8*/4' curve shows an insulator-to-metal transition around 160 K. This further decreased transition temperature is a sign of a further weakened inter-grain magnetic coupling. Accordingly, the inter-grain MR value of the sample is enhanced by a factor of two as compared with that of the undoped partner grown under similar conditions. Careful inspection of the deposition conditions of the two series reveals that the different behaviours of the two samples, '8/4' and '8*/4', can be attributed to the smaller separation between the two laser spots on the manganite and Ag target in the T_s-varying series. Moreover, we note that the deposition T_s of the former may be slightly higher.

In order to reveal the origin of the enhanced MR in the above-mentioned Ag-doped film, labelled as '8*/4', TEM was employed to study the microstructures. The planar section TEM image of the sample is presented in figure 5. The inset shows the corresponding electron diffraction pattern. The figure reveals 'clusters' of 100–150 nm, each consisting of hundreds of sub-grains of 10–20 nm—similar to the size of the ordinary columns in the undoped sample. An amorphous zone about 5–10 nm wide exists among these clusters. The electron diffraction shows a diffusive amorphous halo in addition to the ring-like distributed polycrystalline reflections, which suggests that the amorphous fraction in the film is remarkable. It is obvious that the amorphous phase also exists at the sub-grain boundaries, and seems to 'glue' the nano-sized sub-grains into larger clusters. The fitting results for this sample are also listed in table 1. The very large ρ_{c0} suggests a very poor crystallinity even inside the grains, and the $m\%$ value is very low because in this sample the crystalline grains are almost embedded in amorphous phase.

During film deposition, because the two laser spots were very close to each other, they 'interacted'. That is, the species ablated from the LSMO target collided with the ablated Ag atoms, and lost part of their kinetic momentum. Therefore during film deposition the LSMO adatom condensation on the substrate was interrupted by the heavy Ag precipitation; as a consequence, the formation of amorphous phase is enhanced. This is in fact consistent with the previous observation of the anomalous larger grains in the Ag-doped films, which are believed to have a similar structure to the clusters in this sample. It is then easy to understand the increase in content of these anomalous grains with increasing Ag precipitation. It is reasonable to claim

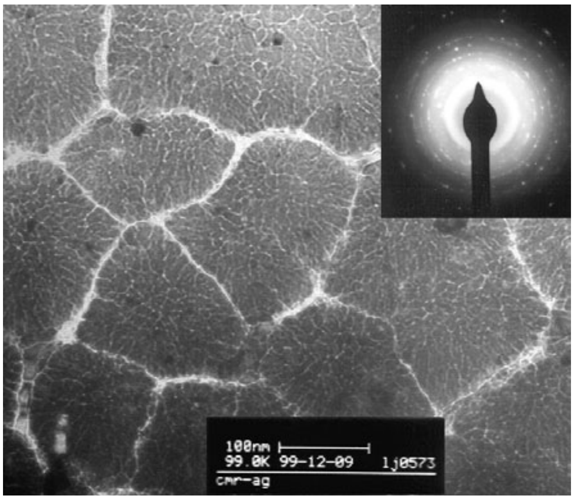

Figure 5. The planar section TEM image of the Ag-doped film shown in figure 4(a), labelled '8*/4'. Clusters around 100 nm consisting of nano-sized crystalline phase and amorphous phase are shown. The inset shows the corresponding selected-area electron diffraction pattern.

that Ag exists at the boundary zones among grains and the sub-grain boundaries inside the clusters, and enhances the formation of the amorphous phase. The amorphous phase increases the magnetic spin disorder at the interfaces, serves as scattering centres, and thus increases the low-temperature inter-grain MR value.

4. Conclusions

In summary, Ag atoms inside LSMO grains diffuse to grain boundaries and are separated out as a metallic Ag phase among LSMO grains. The diffusion of Ag catalyses the grain boundary diffusion of LSMO species, and thus changes the shape of the polycrystalline columns into closely arranged polyhedra. The in-plane alignment of the film is improved and a better grain boundary ordering is achieved. In other words, the effective sections of the conducting channel, where crystalline grains are connected by small-angle grain boundaries, are increased upon Ag doping. Therefore the sample resistance is reduced and the inter-grain MR at low temperatures is suppressed. On the other hand, by means of the DBPLD method, at an appropriate Ag precipitation level and under carefully adjusted deposition conditions, the laser plumes of the two targets can be caused to interact with each other and favour the formation of amorphous phase among the grains. A cluster structure consisting of nano-sized crystals surrounded by amorphous phase with a fairly high activation energy can then be obtained, where an inter-grain MR enhancement is observed. This enhanced MR is attributed to the magnetic spin disordering at the interface of the crystal and amorphous phases.

Acknowledgments

The authors thank Z W Li, S G Wang, and Y J Zhang for fruitful discussions.

References

[1] Moshfegh A Z, Wang Y Q, Sun Y Y, Mesarwi A, Hor P H and Ignatiev A 1993 *Physica* C **218** 396
[2] Kalyanaraman R, Oktyabrsky S and Narayan J 1999 *J. Appl. Phys.* **85** 6636
[3] Xu S Y, Ong C K, You L P, Li J and Wang S J 2000 *Physica* C **341** 2345
[4] Shreekala R *et al* 1999 *Appl. Phys. Lett.* **74** 2857
[5] Li J, Huang Q, Li Z W, You L P, Xu S Y and Ong C K 2001 *J. Phys.: Condens. Matter* **13** 3419
[6] Li J, Huang Q, Li Z W, You L P, Xu S Y and Ong C K 2001 *J. Appl. Phys.* **89** 7428
[7] Tao T, Cao Q Q, Gu K M, Xu H Y, Zhang S Y and Du Y W 2000 *Appl. Phys. Lett.* **77** 723
[8] Ong C K, Xu S Y and Zhou W Z 1998 *Rev. Sci. Instrum.* **69** 1
[9] Thompson N R 1973 *The Chemistry of Copper, Silver, and Gold* (Oxford: Pergamon)
[10] Murch G E and Nowick A S 1984 *Diffusion in Crystalline Solids* (New York: Academic)
[11] Liu J M, Ji L, Huang Q, You L P, Wang S J, Ong C K, Wu Z C and Liu Z G 2000 *Appl. Phys. Lett.* **76** 2286
[12] Gupta A, Gong G Q, Xiao Gang, Duncombe P R, Lecoeur P, Trouilloud P, Wang Y Y, Dravid V P and Sun J Z 1996 *Phys. Rev.* B **54** 629
[13] Li X W, Gupta A, Xiao Gang and Gong G Q 1997 *Appl. Phys. Lett.* **71** 1124
[14] Lee S, Hwang H Y, Shraiman B I, Ratcliff W D and Cheong S W 1999 *Phys. Rev. Lett.* **82** 4508
[15] Walter T, Dörr K, Müller K H, Holzapfel B, Eckert D, Wolf M, Schlfer D and Schultz L 1999 *Appl. Phys. Lett.* **74** 2218
[16] de Andrés A, García-Hernández M, Martínez J L and Prito C 1999 *Appl. Phys. Lett.* **74** 3884
[17] de Andrés A, García-Hernández M, Muñoz-Martín A, Martín L, Prito C and Martínez J L 2000 *Thin Solid Films* **373** 97
[18] Salamon M B and Jaime M 2001 *Rev. Mod. Phys.* **73** 583
[19] Snyder G J, Hiskes R, DiCarolis S, Beasley M R and Geballe T H 1995 *Phys. Rev.* B **53** 14 434
[20] Han K H, Huang Q, Ong P C and Ong C K 2001 *J. Phys.: Condens. Matter* **13** 8745